Design of a High-Temperature, Power-Constrained Electrified District Heating Network with Thermal Storage and Curtailed Wind Integration

Design of a High-Temperature, Power-Constrained Electrified District Heating Network with Thermal Storage and Curtailed Wind Integration

Thibaut Desguers*, Daniel Friedrich

School of Engineering, Institute for Energy Systems, The University of Edinburgh, United Kingdom

Abstract

The electrification of heating, and in particular district heating networks, is challenging from system integration and cost perspectives but could provide significant services for the wider electricity system. In this work, several control strategies are compared for the optimal design of a high-temperature, power-constrained electrified district heating network of a university campus with borehole thermal energy storage and grid services such as flexibility, load-levelling and wind curtailment mitigation. The proposed heat plant operation is modelled in TRNSYS and its performance is analysed from a grid operator and end-user's viewpoint. The impact of several system parameters is investigated in a sensitivity analysis.

It is shown that, depending on the control strategy, total efficiencies up to 200 % and curtailed wind fractions up to 43.8 % are achievable with great flexibility and load-levelling, and operating costs and emissions significantly lower than for gas-reliant systems. A control strategy which aims for load-levelling and maximal storage headroom is shown to be best suited from the perspective of both the end-user (efficiency, emissions and cost) and grid operator (grid services). A compromise between efficiency and grid services is highlighted which could be mitigated by financial incentives for curtailed wind integration, benefiting both consumers and grid operators.

Keywords: District Heating; Electrification; Thermal Storage; Curtailed Wind Mitigation; Power Constraint

NOMENCLATURE

Acronyms & Abbreviations

ASHP	Air Source Heat Pump
BTES	Borehole Thermal Energy Storage
CHP	Combined Heat and Power
COP	Coefficient of Performance
DHN	District Heating Network
DNO	Distribution Network Operator
ESO	Energy System Operator
GB	Great Britain
GBp	Pence (hundredth-division of British currency)
HP	Heat Pump
HX	Heat Exchanger
KB	King's Buildings
MFR	Mass flow rate
S1, S2, S3	Operation Controller Strategy 1, 2 & 3
SOC	State of Charge
STS	Short Term Storage

*Corresponding author

Email address: thibaut.desguers@ed.ac.uk (Thibaut Desguers)

UK United Kingdom

WF Curtailed Wind Fraction

Symbols

ΔP Pressure losses (Pa)

δT_d Temperature difference threshold for BTES controls (°C)

$\dot{m}$ Mass flow rate (kg/s)

$\dot{m}_0$ Rated mass flow rate (kg/s)

$\dot{Q}_e$ Heat pump electrical consumption (W_e)

$\dot{Q}_{th}$ Heat pump thermal output (W_{th})

ϵ Pipe roughness (m)

η_{BTES} Annual BTES recovery rate (-)

η_{th} Electricity-to-heat thermal efficiency (-)

η_{tot} Overall thermal efficiency (-)

γ_h Heater load (-)

ρ Fluid density (kg/m^3)

c_p Specific heat (J/kg/K)

D Pipe diameter (m)

E_{demand} Total annual heat demand (Wh)

$E_{el,heat}$ Annual heat demand (Wh)

$E_{el,h}$ Annual electrical consumption of the heater (Wh)

$E_{el,in}$ Total annual conbined electrical consumption of the heat pumps and electric boiler (Wh)

$E_{el,pumps}$ Total annual electricity consumption of the pumps (Wh)

$E_{th,BTES}$ Annual amount of thermal energy charged into the BTES (Wh)

f Darcy fricton factor (-)

L Pipe length (m)

P_0 Constant for COP equation (kW)

P_{HP} Heat pump electrical capacity (W)

P_{max} Annual peak thermal demand (W_{th})

R_e Reynolds number (-)

T_0 Constant for COP equation (K)

T_r DHN return temperature (°C)

T_s DHN target supply temperature (°C)

$T_{BTES,CTR}$ Average temperature in the vicinity of the cental borehole (°C)

$T_{BTES,MAX}$ Maximum allowed BTES temperature (°C)

$T_{cond,in}$ Working fluid temperature at heat pump's condenser inlet (°C)

$T_{cond,out}$ Working fluid temperature at heat pump's condenser outlet (°C)

T_{source} Temperature of the heat source (ambient temperature) (°C)

$T_{STS,TOP}$ Average temperature in the upper 20 % STS volume (°C)

1. Introduction

In Scotland in 2020, heat accounted for 52.9 % of all energy consumption, of which only 6.5 % came from renewable sources, accounting for 19.25 % of all Scottish greenhouse gas emissions [1]. Therefore, decarbonising the heating sector is an essential step towards achieving net zero goals in Scotland and the UK.

Provided that the electricity supply is decarbonised, the electrification of heat is a possible solution; in Scotland in 2020 for example, 98.4 % of the gross electricity consumption came from renewable sources [1]. In particular, District Heating Networks (DHN) with seasonal or long-term

thermal energy storage charged through solar thermal, industrial waste heat or otherwise curtailed electricity could provide a valuable contribution to the decarbonisation of heating (see solar district examples in the UK [2] and Chile [3]) and, when linked to the operation of the electricity system, to the wider energy system as well [4]. Hydrogen is another low-carbon option, however it has been shown to be too costly and inefficient for the decarbonisation of space heating [5] and is therefore more valuable for hard-to-decarbonise sectors such as aviation and heavy industry.

Renewables often produce an unpredictable, fluctuating and intermittent energy supply which does not coincide with peaks of demand, and energy storage is needed to bridge the gap and decouple energy production from demand. Besides, high penetration of renewables into the energy mix also constitutes a great challenge for the transmission and distribution networks, often resulting in large amounts of renewable energy being increasingly curtailed due to network constraints or a temporal mismatch with demand [6]. In the UK in particular, curtailment levels of wind energy could reach up to 86 TWh by 2036 according to the National Grid ESO [7], equivalent to 22 % of the total UK electricity demand predicted for that year. Therefore, a renewable capacity increase must be accompanied by the simultaneous development of flexibility options including demand-side flexibility and large-scale inter-seasonal energy storage [7], for which the main options are hydrogen and thermal energy storage.

To increase flexibility and, as recommended by the National Grid ESO to mitigate wind energy curtailment [7], in this work long-term thermal energy storage is incorporated into the heat-plant design. Specifically, subsurface Borehole Thermal Energy Storage (BTES) is considered which is a well-known storage technology [8–12] with many operational installations worldwide (for example in Denmark [13], Canada [14], and Germany [15]) and advanced numerical modelling tools (for example the thermal resistance and capacity model [16], which can be integrated in a 1D line elemt coupled with a 3D finite element mesh [17], a full finite element formulation [18], or a 1D model of the heat transfer fluid coupled with a 2D ground model [19]), including a module in TRNSYS[1] [20], the modelling software used in this study. BTES installations allow heat to be stored in the ground and recovered by circulating a heat transfer fluid through an array of borehole heat exchangers, relying on thermal conduction to exchange thermal energy with the surrounding soil.

To address the issues of domestic heat decarbonisation and curtailment of wind energy in the UK, in this work the design of a high-temperature, power-constrained electrified heat plant with curtailed wind utilisation and integrated BTES thermal energy storage is investigated. The University of Edinburgh, which has a pledged to be carbon neutral by 2040, and in particular its King's Buildings (KB) campus in Scotland, is taken as a case study. The layout and controls of the heat plant are optimised for the decarbonisation of KB's DHN, which is currently fully reliant on natural gas through the joint operation of a Combined Heat and Power (CHP) unit and gas boilers. The electrification of heat at KB, with all fossil fuel based heat generation decommissioned, is subject to the following constraints:

- Restricted grid connection: this requires careful design and operation so that the heat demand is met at all times
- High supply temperature (in excess of 85 °C in winter): a lower temperature 4^{th}- or 5^{th}-generation DHN would require significant and prohibitively expensive and time-consuming building retrofit. A high-temperature electrified DHN is therefore considered
- Curtailed wind energy utilisation: the heat plant is design to respond to and mitigate wind curtailment

[1] https://sel.me.wisc.edu/trnsys/

This case is representative of old or protected buildings in the UK with restricted retrofitting permissions, and is therefore chosen to identify and illustrate the complexities and challenges of cases of constrained heat electrification. The design of a temperature and power constrained electrified heat plant with BTES storage for curtailed wind integration has, to the author's knowledge, not been done before. Finally, the effects of different parameters (*e.g.* supply and return temperature) on the consumer, grid operator and on the use of otherwise curtailed wind electricity are also investigated. The results are presented and analysed from both a consumer's and grid operator's viewpoint.

2. Methods and case-study

In this section, the methods for the modelling and optimisation of the different components of the system are outlined, including a description of the KB campus and the proposed heat plant, the BTES controls and Operation Controller strategies, the required input data and the optimisation procedure.

2.1. Case study: KB campus

KB is situated across two thin and fractured aquifers which are unsuitable for open-loop aquifer thermal storage, however the rock formations are well suited for closed-loop BTES. The ground properties are reported in Table A.1 (provided as supporting information) along with all BTES parameters.

KB is a large campus which currently operates a 2.7 MWe CHP unit together with three 7 MWth gas boilers coupled with a 150 m^3 hot water thermal buffer tank to meet its thermal demand. A difficulty in the electrification of heat at KB lies in its high DHN supply temperature which is in excess of 85 °C in winter, belonging to the 3^{rd} DHN generation. Recently, there has been a push for lower-temperature DHNs through the development of 4^{th}- and 5^{th}-generation DHNs with supply temperatures around 50-60 °C and ambient, respectively (see [21] for the definition of 4^{th}-generation district heating, [22] for a review of existing 5th-generation system operating in Europe, and [23] for 4^{th} and 5^{th} generation district heating and cooling networks). Lower supply temperatures allow the use of multiple renewable heat sources such as solar thermal, geothermal, seawater and industrial waste heat, a more efficient use of energy resources and better integration of renewable energy [24]. They also lead to greater energy efficiency (higher Coefficients of Performance (COP) for electrified heating systems with incorporated heat pumps, reduced transportation losses in pipes [24]), and lower fossil fuel energy consumption, heat losses and cost of heat [25], however retrofits are required to not reduce thermal comfort [26], among other benefits, therefore assisting with the decarbonisation of the heat sector as a whole. However today most buildings, including KB, are designed for supply temperatures above 70 °C and low-temperature DHNs are more suitable for new energy-efficient builds [25]. A reduction of the supply temperature in existing 3^{rd} generation DHNs would require significant low-temperature retrofits to the buildings, such as replacing radiators [27] and windows [26**?**] which, in KB's case, would constitute a significant, costly and time-consuming challenge. Therefore in this work, a high-temperature ($\geq$ 65 °C) electrified DHN is studied and the effect of lowering the supply temperature down to 55 °C is investigated.

The proposed heat plant relies on the electrification of heat through the use of heat pumps together with back-up electric heaters, and with the CHP and gas boilers decommissioned. KB has no access to a large enough water source so that air-source heat pumps (ASHP) are the most suitable option. The heat plant design and operation are optimised to provide demand-side response grid services such as flexibility, load-levelling and integration of wind energy which would otherwise be curtailed. However, this requires an additional electrical

connection to the distribution network (on top of KB's already-existing 5 MWe connection) which in KB's area is restricted to a firm (resp. non-firm) 6 MWe (resp. 12 MWe) capacity, and the former is used in this work. Consequently, judicious control strategies are needed, and several options are explored in this study.

2.2. Heating system design and modelling

All modelling in this study is performed in TRNSYS. A schematic from TRNSYS' graphical interface of the proposed heating system layout is shown in Figure 1a. In line with the university's net-zero pledge, the operation of the CHP and gas boilers is discontinued, and heat is generated primarily by an ASHP which is complemented by a back-up kettle-style electric heater. The electric heater is immersed in the short-term storage (STS) tank, which is the central hub connecting the different parts of the system. In particular, the STS tank is needed to buffer heat generated from otherwise curtailed wind because the BTES has a lower charge rate which restricts the amount of otherwise curtailed energy which could be directly charged into the BTES. The BTES, whose operation is regulated by the "BTES Controller", is charged by the ASHP or STS tank and discharges into the return line of the DHN, represented by the pink / purple loop on the schematic. The "Operation Controller" regulates grid imports based on the strategy of operation, the current curtailed wind and electricity market conditions and other system variables such as local temperatures and heat demand.

The heat plant comprises five main loops, and is almost identical to another heat plan described elsewhere [28]. The only difference is that a kettle-style electric heater (Type 1226 in TRNSYS) immersed in the STS tank is used in place of a separate electric boiler unit. All relevant system parameters are provided elsewhere [28], and are provided as supporting information in Table A.1. In particular, the COP of the ASHP is described by the following equation [28]:

$$COP = 1.6244 \times \ln\left[\frac{P_{HP}}{P_0}\right] \times \exp\left[-\frac{T_s - T_{source}}{T_0}\right] \quad (1)$$

where $P_0 = 1.87$ kW and $T_0 = 42.83$ K are constants, P_{HP} is the ASHP erated electrical capacity, T_s is the DHN supply temperature (ASHP condenser outlet temperature), and T_{source} is the temperature of the ASHP heat source (ambient air in the present case). Equation 1 is graphically shown in Figure 2 for typical operating conditions encountered under the Operation Controller strategies presented in section 2.4. It clearly shows the benefit of lower DHN supply temperatures and larger ASHPs; for example, each 10 °C drop in DHN supply temperature is accompanied by a 26.3 % rise in COP, and a sixfold increase in P_{HP} yields a 28.5 % COP increase.

2.3. System operation: BTES layout and controls

Historically, BTES installations of two main types have been commonly used; near-ambient temperature BTES for combined heating and cooling [9], and high-temperature BTES for heating only [10]. In the former case, cooling is provided in summer by extracting heat and charging it into the BTES, while space heating is provided in winter by discharging the BTES. In the latter, the BTES is usually charged from seasonal solar energy or industrial waste heat [11] in summer, and discharged into a low-temperature DHN for space heating in winter, typically between 45 °C and 55 °C. BTES charging temperatures vary among installations, and maximum storage temperatures typically range from 45 °C to 75 °C (see, for example, a high [14] and low [29] temperature case). Additionally, a BTES array may be used in conjunction with a heat pump at its outlet to address seasonal imbalances in ground temperatures in the first case, or to raise its discharge temperature and therefore raise the grade of extracted heat in the latter.

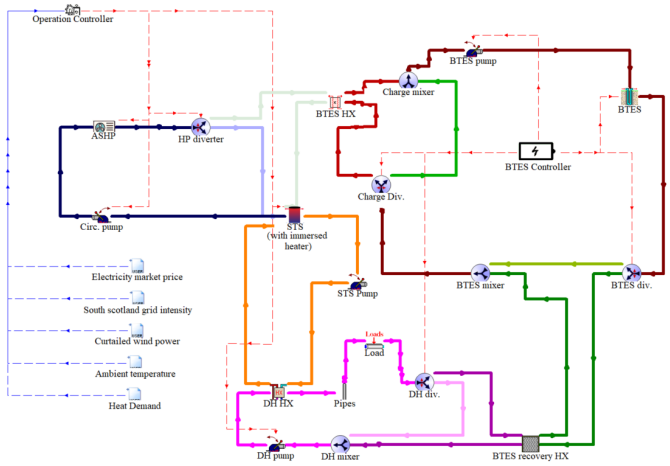

(a) Schematic of energy system design. For clarity, only the main components and connections are shown. Solid lines indicate fluid pipes, and dashed lines indicate input (blue) or command (red) signals. Within a given loop, identical colours indicate identical flow rates. There are 4 main loops: STS loop (orange), ASHP loop (blue), Load loop (pink & purple), and BTES loop (green & brown

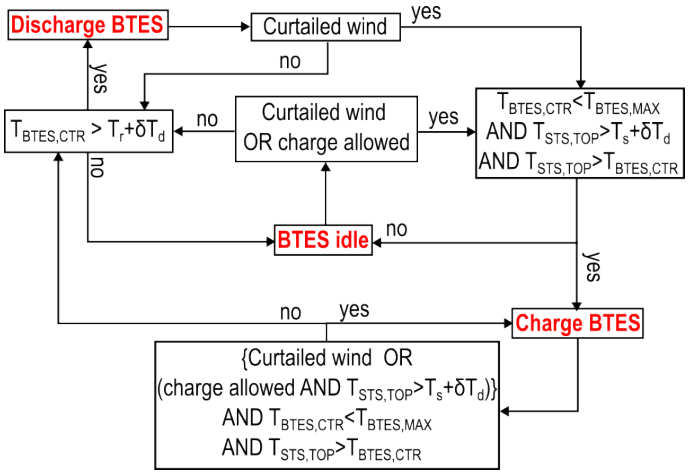

(b) BTES charge and discharge decision tree (from [28]). See the NOMENCLATURE for symbols and variables

Figure 1: TRNSYS system schematic and BTES decision tree

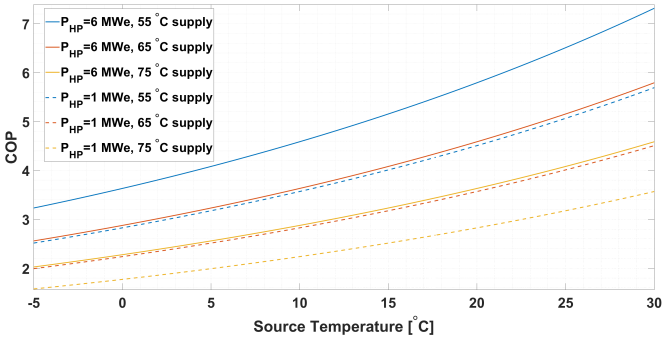

Figure 2: ASHP operating map: COP as a function of source temperature for seeral DHN supply temperatures and ASHP rated electrical power

However in the present case, grid access is restricted to 6 MW (see section 2.6) which is 1.6 times lower than P_{max}; therefore, any heat pump placed downstream of the BTES would reduce the system's electricity-to-heat generation capacity and compromise its ability to meet demand peaks, and this option is dismissed. Besides, typical charge and discharge rates for BTES installations are 50 - 70 W per meter of borehole length; with the parameters listed in Table A.1, maximum rates of order 740 - 1,000 kW can be expected which remains small compared to KB's peak winter demand of 9,620 kW (see section 2.5). Also, feeding the BTES outlet into the DHN supply line would require the ground to be charged up to temperatures higher than T_s, which is in excess of 85 °C at KB in winter. This is difficult to achieve as the charging process would be lengthy and inefficient due to increased thermal losses, and the BTES availability to discharge and the discharge power would be limited in time and magnitude, respectively. Such a set-up was investigated in TRNSYS and showed that the BTES brought a negative contribution to the system's overall efficiency and cost.

In light of all these considerations, it was chosen to connect the BTES to the DHN return line, which effectively raises the grade of the energy extracted from the BTES as it increases both the discharge power and stored heat availability (both due to lower heat sink temperatures). However this raises the DHN return line temperature downstream of the load which requires higher temperatures in the STS tank and increases thermal losses.

The BTES controller decision tree which regulates the BTES charge and discharge cycles is represented in Figure

1b, and was built into a custom module in TRNSYS. In the simulation, the discharge threshold δT_d and the maximum allowed BTES temperature $T_{BTES,MAX}$ are set to 2 °C and 95 °C, respectively. The BTES is only charged with curtailed wind energy, either directly when it is currently available ("Curtailed wind" = "yes" in Figure 1b), or indirectly through STS discharge after a wind curtailment event until it is fully depleted ("charge allowed" = "yes", in which case no extra energy is allowed to be imported from the grid).

The decision tree and flow routing during BTES charge and discharge phases are described elsewhere [28] in more detail.

2.4. System operation: Operation Controller strategies

Three different Operation Controller strategies have been explored and are explained below. They are represented in graphic form in Figure 3.

2.4.1. Strategy 1 (S1)

In this control strategy, the Operation Controller mainly seeks to follow the thermal demand in real time, except during wind curtailment events where it operates the heat plant at full capacity to maximise curtailed wind utilisation. Following a wind curtailment event, all electricity imports from the grid are held off until either the STS has been fully depleted by discharging into the DHN, or another wind curtailment event happens, whichever is first. Outside wind curtailment events, when grid imports are allowed, only as much energy as is necessary for the current timestep is purchased, except if $T_{STS,MAX} < T_s$ in which case the plant operates at full capacity until $T_{STS,MAX} > T_s + 1$ as an emergency measure.

This strategy was chosen for several reasons;

- it is easy to implement
- it is a simple way to meet the load at all times while integrating curtailed wind energy
- since the heat generation plant is run at minimal capacity outside wind curtailment events, the STS average SOC is likely to be low which increases the headroom available for curtailed wind energy integration

However one drawback is that this strategy leaves minimal leeway for demand-shifting as the plant's electrical demand is likely to have a similar profile as the heat demand, *i.e.* highly variable at daily, weekly and seasonal timescales, thereby mitigating the overall benefit to the grid operator. Besides, from a consumer perspective, the associated running costs and emissions are expected to be relatively high as grid imports are likely to coincide with periods of high nationwide demand, which are usually linked to increased energy production costs and emissions as more fossil fuel generators are needed.

2.4.2. Strategy 2 (S2)

In an attempt to flatten the heat plan electrical demand curve and provide demand-shifting services to the grid, in this strategy the daily heat demand is averaged over six hour windows, yielding four distinct levels per day, which serves as a baseload generation target for the plant. At each timestep, any generation in excess of the current demand is stored in the STS tank, and any generation deficit is compensated by an energy discharge from the STS (where this is not possible, the plant output is increased accordingly, inevitably introducing spikes in the electrical demand). During and following wind curtailment events, the system operation is the same as with S1. This strategy is expected to yield flatter electrical demand curves.

Note that implementing this strategy in practice requires the heat demand to be known a day ahead. Prediction models are beyond the scope of this work and, without one, the actual heat demand profile is used.

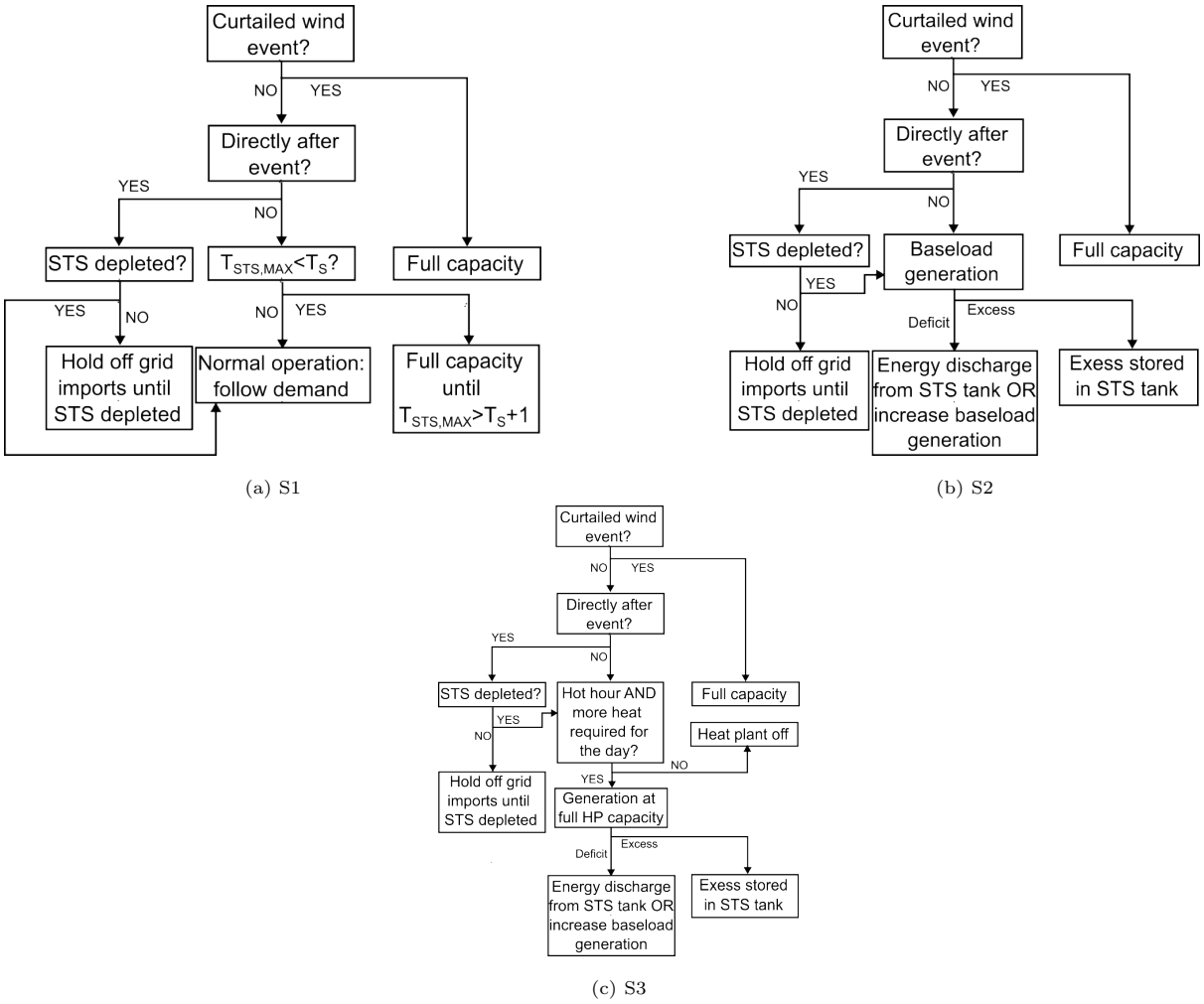

(a) S1

(b) S2

(c) S3

Figure 3: Graphical representations of Operation Controller strategies

2.4.3. Strategy 3 (S3)

In an attempt to boost the ASHP COPs, in this strategy the ASHP is run during the hottest hours of the day as a priority. At the start of each day, the total heat demand for the day is calculated, the COPs predicted based on weather forecast data, and the heat pumps are run at full capacity during the hottest hours of the day (with no electric heater input) for a number of hours large enough in order to produce the required amount of heat for the day. Wind curtailment events and generation excesses and deficits are handles in the same way as with S2.

This strategy is expected to yield larger thermal efficiencies and thus reduce operational costs, and would therefore be beneficial primarily to the consumer, while load-shifting is likely to be less efficient than with S2.

2.4.4. All cases

In all cases and strategies, the heat pump outlet temperature $T_{cond,out}$ is set to a fixed value (which is an optimisable variable, see section 2.6) and its mass flow rate is adjusted to produce the required amount of heat. Priority is given to the heat pump over the electric heater as it is more thermally efficient. Finally, when the heat plant operates at full capacity, care is taken to not exceed the STS and BTES maximum allowed temperatures, which may require adjustments to the heat plant output.

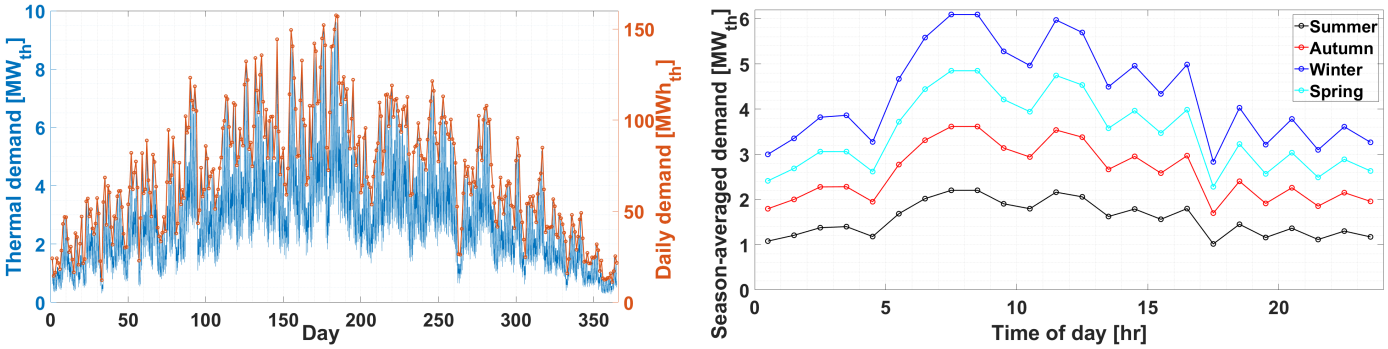

(a) Time series, 8th August 2018 - 8th August 2019

(b) Season averaged daily profiles

Figure 4: KB's thermal demand profile

2.5. Input data

2.5.1. Thermal demand profile

An hourly time series for KB's thermal demand was provided by the University of Edinburgh based on meter readings for a period covering 8th August 2018 - 8th August 2019. At the time of recording, a total of 31 buildings were connected to the campus' DHN including a nursery, a library, teaching and study spaces, offices and several laboratories.

The time series is shown in Figure 4a along with the daily energy totals. It exhibits a strong seasonal pattern with a yearly peak at 9.62 MWth in winter for a total energy of 157.52 MWh for that day and 26.17 GWh over the whole year. The demand exceeds the 6 MW grid-connection restriction for 5.39 % of the year.

The profile also shows a clear weekly pattern consistent throughout the year with higher demand on weekdays, along with a daily pattern as shown in Figure 4b. The season-averaged daily profiles have a consistent shape across all seasons with two well-defined peaks centred around 8 am and 11.30 am and lower levels at night. The demand is lowest in summer, followed in increasing order by autumn, spring and winter.

2.5.2. Curtailed wind time series

Half-hourly wind curtailment data were extracted from the National Grid Elexon's portal [30] for 10 selected wind farms in southern Scotland and are available online [31].

With no clear temporal pattern, it shows 184 wind curtailment events for a total of 1508 hours throughout the year (*i.e.* a cumulative 62.83 days, or 17.21 % of the year), and with a peak power of 1,572 MW. The duration of events ranges from 30 min to 76.5 hours, with a mean (resp. median) of 8.2 hours (resp. 4 hours). The spacing between events ranges from 30 min to 527 hours (*i.e.* 21 days 23 hours), with a mean (resp. median) of 39.4 hours (resp. 13.75 hours).

These numbers show great variability and inconsistency in magnitude and frequency of curtailed wind events, which highlights the complexity in integrating it into energy systems. There is enough yearly curtailment to meet KB's annual thermal demand in full, however large thermal stores would be required to accommodate its temporal variability. Therefore, the optimal heat plant design is expected to result from a compromise between goal, technical feasibility and cost, and requires a control strategy to be built accordingly, as set out in section 2.4.

It is worth pointing out that KB's use of curtailed wind energy will only have a very small impact on the levels of wind curtailment at a national scale. KB's electricity demand for heating is less than 0.01 % of Great Britain's (GB) electricity demand and less than 1 % of the peak curtailment. On the other hand, the proposed system could be replicated at dozens or even hundreds of sites across GB, at which point it would have a significant impact and

the interactions would need to be considered.

2.5.3. Other data

Half-hourly data for the grid carbon intensity in southern Scotland are available online [32], and show an average value of 35.43 gCO2/kWh over the year (the impact of KB's required extra 6 MW connection on other UK sub-grids is not taken into account).

The electricity retail price used in this study is based on the 2018 Octopus Agile tariff. It follows the wholesale day-ahead market price and its daily and seasonal variations, with a cap at 35.00 GBp/kWh. Data are openly accessible online [33]. It has a mean (resp. median) value of 11.35 GBp/kWh (resp. 9.66 GBp/kWh).

2.6. Optimisation

For the optimisation process, a total of three optimisable variables are used, and eight output metrics are calculated. All are defined in Table 1. Note that, in order to focus the analysis on the control strategies and technical challenges related to constrained heat generation, the BTES size and associated parameters are fixed in this study. Also, the economics of the suggested electrified heat plant is made complex by the integration of curtailed wind, for which no market mechanism or financial incentives yet exist. A financial analysis of such a heat plant, which quantifies the benefits of curtailed wind integration with BTES, requires a separate detailed study of its own, and is presented elsewhere with BTES parameters as optimisable variables [28].

Combining all optimisable variables, a total of 108 scenarios are run in TRNSYS for each strategy, coming to 324 scenarios altogether, each with a 10-min timestep. At the start of each simulation, all temperatures are set to 10 °C and all stores are empty. The only constraint in the optimisation process is the 6 MW grid connection as per DNO restrictions in KB's area. It is worth mentioning that KB's electricity demand is covered by a 2.8 MWe CHP unit complemented by an already existing 5 MW grid connection. However the 5 MW connection is never fully used, and is assumed large enough to cover the electrical demand of the heat plant's pumps. Therefore, the 6 MWe restriction applied to the ASHP and electric heater only.

Due to the ground's thermal inertia, it takes a few years for the system to reach full temperature and stable operation, during which time the system's outputs vary significantly. In the Drake Landing example [14], the BTES efficiency (and associated solar fraction) is predicted to take 8 years to stabilise, which agrees well with measured data. This is consistent with the results presented in Table 2 which show that after 8 years of operation, the year-on-year relative change in average BTES temperature drops below 0.02 %. As a result, to best characterise the system's performance, all the results and subsequent analyses presented below are given for stable operation, which is considered to happen from the 8^{th} year onward. Therefore all simulations are run for 8 years with no preheating (*i.e.* the BTES controller and Operation Controller operate in the same way each year, and all input data are the same each year too), and all output metrics are calculated for the final year.

All results are analysed from a consumer and grid operator perspective in the next section below.

3. Results and discussion

In this section, the results are presented and discussed qualitatively in subsection 3.1, and quantitatively analysed from a grid operator and user perspective in subsection 3.2. A sensitivity analysis is then performed in subsection 3.3.

3.1. System performance

For each control strategy and target DHN supply temperature, results are presented for three $T_{cond,out}$ levels ($T_s + 5$ °C, $T_s + 10$ °C and 95 °C) in Table 3. In all cases,

Name	Symbol	Definition & Comments
Optimisable variables		
Supply temperature	T_s	[55,65,75] °C with return temperature $T_r = T_s - 20$
ASHP outlet temperature	$T_{cond,out}$	From $T_s + 5$ to 95 °C in 5 °C increments
		Also maximum allowed STS tank storage temperature
ASHP	-	Rated electric powers between [1,6] MWe
		Electric heater utilisation depends on heat plant output and ASHP utilisation
Output metrics		
Curtailed wind fraction	WF	Proportion of the heat plant's electrical consumption covered by otherwise curtailed wind energy
		Defined as percentage of purchased electricity which would otherwise have been curtailed
Thermal efficiency	η_{th}	$\eta_{th} = \frac{E_{demand}}{E_{el,heat}}$
		Thermal efficiency of the electricity-to-heat process (excluding pupming)
Overall thermal efficiency	η_{tot}	$\eta_{tot} = \frac{E_{demand}}{E_{el,heat}+E_{el,pumps}}$
		Overall thermal efficiency (including pumping)
Heater load	γ_h	$\gamma_h = \frac{E_{el,h}}{E_{el,heat}}$
		Share of electric heater in heat generation
BTES charge	$E_{th,BTES}$	Annual amount of thermal energy charged into the BTES
BTES recovery rate	η_{BTES}	Annual proportion of thermal energy recovered from the BTES
Operational costs	-	Annual costs for the heat plant electrical consumption
Emissions	-	Equivalent CO2 emissions per unit heat generated by the heat plant

Table 1: Optimisable variables and output metrics. All symbols and their units are defined in the Nomenclature

a 6 MWe ASHP yielded the largest WF and thermal efficiencies, so that no results are presented for other sizes.

For gas, metered data from KB shows an 85.0 % thermal efficiency for the gas boilers (the CHP unit currently in operation at KB will be decommissioned within the next few years, so that only boilers are considered for comparison purposes). The associated emissions are calculated based on the carbon content of natural gas, 202.0 gCO2/kWh [34], which is then divided by the thermal efficiency, giving 237.6 gCO2/kWh. In 2018, KB was paying 6.2 GBp/kWh of gas which, divided by the thermal efficiency, gives an equivalent fuel cost of 7.3 GBp/kWh of heat. Note that for lack of data on pumps, these numbers do not include emissions or costs associated with boiler pumps and are therefore underestimates.

In all cases, the WF associated with the total heat plant electrical consumption is lower than for heat generation only since the pumps operation, in particular the STS, DH and BTES pumps, is generally independent of curtailed wind availability. For S1 and S2 at a given T_s, the WF increases with increasing $T_{cond,out}$, for two reasons. $T_{cond,out}$ is also the maximum allowed STS temperature, resulting in larger STS storage capacities at higher levels, and therefore larger storage headroom and curtailed wind energy integration. Also for a given ASHP thermal output $\dot{Q}_{th}$, reduced COP values at elevated temperatures require larger electrical power ($\dot{Q}_e$) values, and therefore larger curtailed wind utilisation. However, this comes with a drop in thermal efficiency (lower COPs). For S3, the WFs are noticeably lower and less variable than for S1 and S2. This is explained by reduced STS headroom for S3 as most of the heat is produced during the hottest hours of the day and stored in the STS tank until it is fully used, whereas with S1 and S2 heat is consumed sooner after being generated. Therefore outside wind curtailment events the STS SOC is higher with S3 (*i.e.* the STS headroom is lower)

Year	BTES yearly-averaged temperature	Year-on-year change
	°C	%
1	47.64	-
2	55.83	2.55
3	56.23	0.12
4	56.41	0.055
5	56.49	0.0257
6	56.62	0.039
7	56.68	0.020
8	56.73	0.014
9	56.76	0.011
10	56.78	0.0062
11	56.82	0.010
12	56.85	0.0083
13	56.84	-0.00070
14	56.87	0.0089
15	56.88	0.0028
16	56.90	0.0071
17	56.92	0.0036
18	56.92	0.00050
19	56.93	0.0048
20	56.93	0.00

Table 2: TRNSYS results for BTES yearly average temperature and year-on-year change (relative to the initial BTES temperature of 10 ∘C) for a 6 MWe ASHP, 6 MWe electric heater, $T_s = 65$ °C supply temperature and $T_{cond,out} = 95$ °C for 20 years of operation.

as shown in Figure A.1 provided as supporting information. As a consequence, the system operates at reduced flexibility and is unable to absorb as much curtailed wind, regardless of T_s and $T_{cond,out}$.

As shown in more detail below, the thermal efficiency η_{th} is mainly dependent on $T_{cond,out}$ with lower values at higher temperatures regardless of T_s, due to reduced COPs and larger thermal losses. Besides, η_{tot} is lower than η_{th} in all cases due to the pumps electrical consumption.

The required heater size ranges from 4.6 MWe to 6.0 MWe, resulting in a total installed electrical capacity excluding pumps in excess of 6 MWe; however at all times, the electrical consumption for heat generation is restricted to 6 MWe. The reason a heater is necessary to complement the operation of the heat pump is that as the STS tank approaches maximum temperature during charge, the temperature of the working fluid at the condenser inlet increases, reducing $T_{cond,out} - T_{cond,in}$, the temperature elevation of the heat transfer fluid in the ASHP condenser. Because the heat pump mass flow rate $\dot{m}$ is limited, the heat pump must be operated at partial capacity and its electrical consumption $\dot{Q}_e$ must be reduced to not exceed $T_{cond,out}$ at the condenser outlet. The heater can then provide extra heat as necessary, mainly for curtailed wind integration (see section 3.3). The heater load γ_h takes similar values for all three strategies and mainly depends on $T_{cond,out}$, reaching a minimum value at 95 °C. This is explained by reduced COPs at higher temperatures which increases the required HP electricity consumption to achieve a given thermal charge rate, reducing heater usage.

The BTES charge increases with $T_{cond,out} - T_s$ differences regardless of T_s, with similar levels for all strategies, and is due to increased STS and ASHP headroom, resulting in more heat available for BTES charging. Also at fixed T_s, the recovery rate increases with $T_{cond,out}$ as the BTES is then hotter compared to the DHN return temperature (heat sink), boosting the discharge rate and increasing recovery. The recovery rate also rises at lower T_s levels due to reduced thermal losses as the BTES is then colder.

Finally, both the emissions and fuel costs follow the efficiency trends, and are analysed in more detail in the next section below.

3.2. User benefits

In this section, the results are analysed and control strategies ranked from both the grid operator and end-user's perspectives.

3.2.1. Grid operator's perspective: Electrical consumption, flexibility and load levelling

The season-averaged daily profiles for the heat plant's electrical consumption for heat generation is plotted in Figure 5 for maximum WF for all strategies, $T_s = 65$ °C and $T_{cond,out} = 70$ °C.

As expected, the profiles have significantly different shapes

INPUTS			OUTPUTS											
	T_s	$T_{cond,out}$	WF, 6 MWe	WF, Total	η_{th}	η_{tot}	Heater size	γ_h	BTES charge	BTES rec.	Fuel cost, 6 MWe	Fuel cost, Total	Em., 6 MWe	Em., Total
	°C	°C	%	%	%	%	MWe	%	GWh	%	GBp/kWh	GBp/kWh	gCO2/kWh	gCO2/kWh
	75	80	33.6	31.5	200.7	155.2	5.2	16.7	1.4	57.0	7.1	9.0	19.8	24.9
	75	85	35.4	32.8	183.6	144.1	5.1	12.5	1.7	69.9	7.7	9.7	21.7	27.0
	75	95	36	33.3	150.0	122.6	4.9	6.4	1.7	75.1	9.4	11.4	26.7	31.9
	65	70	37.1	33.7	240.8	176.7	5.4	23.1	1.4	70.4	5.8	7.9	16.3	21.6
S1	65	75	39.3	35.2	223.1	165.9	5.3	18.1	1.8	75.8	6.3	8.4	17.7	23.2
	65	95	39.3	35.5	151.6	123.0	4.7	5.4	2.6	81.5	9.3	11.4	26.5	31.8
	55	60	35.2	31.7	263.3	184.9	5.6	37.8	1.4	77.5	5.2	7.4	14.7	20.5
	55	65	39.3	34.5	257.4	181.1	5.4	29.4	1.8	81.8	5.4	7.6	15.1	21.0
	55	95	40.6	36.7	153.4	124.2	4.8	5.8	3.3	87.8	9.1	11.2	26.0	31.4
	75	80	34.3	32.1	201.7	154.6	5.2	15.7	1.4	64.8	7.0	9.0	19.8	25.0
	75	85	36.5	33.7	183.5	143.1	5.1	12.4	1.8	71.4	7.7	9.8	21.8	27.2
	75	95	37.5	34.6	149.5	121.7	4.8	6.2	2.3	76.3	9.5	11.5	26.8	32.2
	65	70	37.7	34.1	243.5	177.3	5.4	21.5	1.4	71.1	5.8	7.8	16.2	21.6
S2	65	75	39.9	35.7	223.1	165.2	5.3	18	1.8	76.6	6.3	8.4	17.8	23.3
	65	95	40.5	36.6	151.2	122.2	4.7	5.3	2.8	82.4	9.3	11.4	26.5	32.0
	55	60	41.7	36.5	289.0	199.8	5.5	28	1.4	77.5	4.8	6.9	13.5	19.0
	55	65	43.8	37.9	266.5	187.4	5.4	24.5	1.8	81.7	5.2	7.4	14.8	20.4
	55	95	43	38.4	153.0	123.0	4.6	4.6	3.1	86.7	9.2	11.3	26.2	31.7
	75	80	31.1	29	206.8	144.7	5.5	13.6	1.3	80	6.6	9.5	19.4	26.7
	75	85	31.6	28.3	192.1	131.9	5.4	12	1.6	83.2	7.2	10.5	20.8	29.1
	75	95	32.6	28.7	158.5	113.0	5.3	8.1	2.2	86.8	9.3	12.7	25.1	33.9
	65	70	34.2	31.1	250.8	166.0	5.6	19	1.3	87.3	5.4	8.2	15.8	23
S3	65	75	34.9	30.2	233.7	151.0	5.3	16.8	1.6	89.1	5.8	9.0	17.0	25.1
	65	95	36.7	31.5	160.8	114.3	5.4	7.3	2.8	92.3	9.2	12.6	24.5	33.3
	55	60	33.4	30.1	271.6	173.0	5.6	35	1.2	94.8	5.0	7.8	14.4	21.8
	55	65	34.3	28.9	260.3	157.8	5.5	30.7	1.5	95.2	5.2	8.6	15.0	23.6
	55	95	33.4	28.7	158.6	110.2	6.0	11	3.4	95.9	9.0	12.7	25.0	34.7
Gas	-	-	0	0	85.9	-	-	-	-	-	7.3	-	237.6	-

Table 3: Summary of results. Each row shows the output metrics for the optimum ASHP size (6 MWe) for given supply and heat pump output temperatures. Emissions and fuel cost for gas do not account for the pumps electrical consumption

for different strategies. Season-wise, all show the same general hierarchy as the demand profiles of Figure 4b. Note that these profiles are season-averaged, and that the hourly time-series show regular electrical consumption peaks of 6 MWe.

With S3, as expected, the profiles closely follow the daily temperature cycles with higher consumption during the hottest hours. However the values never fall to zero, which is partly due to the integration of curtailed wind at all times of day, and partly due to the restricted STS storage capacity which is too small to store a day's worth of heat, even during summer; at 70 °C, the STS storage capacity is 11.6 MWh, *i.e.* only 7.4 % of the peak daily demand. Strategy S3 therefore seems poorly suited for load-levelling.

Strategy S1 shows flatter curves except during winter where significant distortions are visible. Strategy S2 yields similar flat curves, however with significant improvement in spring and winter where most peaks are flattened and the four daily levels become more apparent. In both cases, curtailed wind utilisation results in undulations and fluctuations (see section 3.3).

Therefore in all cases, the curves demonstrate the system's flexibility by its ability to respond to curtailed wind whilst operating as ordered by the Operation Controller. Besides from a load levelling perspective, S2 seems best-suited, especially in spring and winter where the heat demand is highest. Also, the season-averaged profiles show spare electrical capacity and thus potential for more flexibility and curtailed wind integration, which appears to be limited by other factors such as thermal stores capacity and charging / discharging rates.

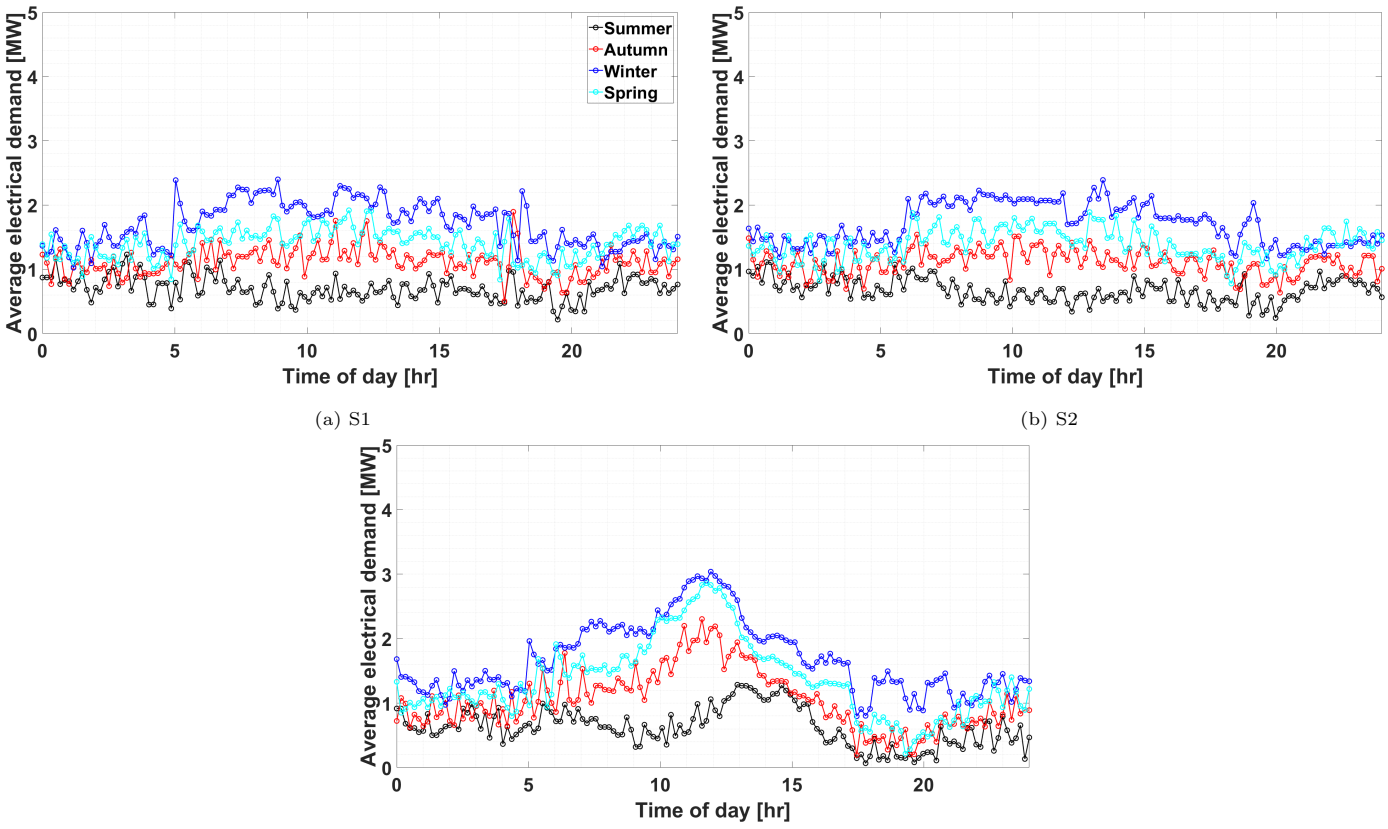

(a) S1

(b) S2

(c) S3

Figure 5: Season-averaged daily profiles for heat plant electrical consumption for heat generation for all strategies, $T_s = 65$ °C and $T_{cond,out} = 70$ °C. The legend is the same for all graphs

3.2.2. Grid operator's perspective: Curtailed wind integration

The WFs (excluding pumping) reported in Table 3 are provided in graphic form as supporting information (Figure A.2).

In all cases, S3 yields the lowest WFs with a maximum of 36.7 %. Besides at lower temperatures ($T_{cond,out} \leq 65$ °C), S2 significantly outperforms S1 while at higher temperatures, both strategies show similar WFs with a slight advantage for S2.

Therefore, S2 seems best suited in terms of curtailed wind utilisation, with up to 43.8 % of the electrical consumption for heat production coming from curtailed wind energy. Together with the load-levelling results, S2 appears to be the best overall strategy from a grid operator's perspective.

3.2.3. Consumer's perspective: Efficiency, operational cost and emissions

The thermal and total efficiencies reported in Table 3 are provided in graphic form as supporting information (Figures A.3 & A.4 provided as supporting information).

Like the WFs, the efficiencies show great variability with values ranging from 149.5 % (resp. 110.2 %) to 289.0 % (resp. 199.8 %) for η_{th} (resp. η_{tot}). As shown in Figure A.3, η_{th} generally decreases with increasing temperature ($T_{cond,out}$ and/or T_s) due to lower COPs, although this may be mitigated by a drop in heater load. As expected, S3 yields the highest η_{th} for $T_{cond,out} \geq 70$ °C with a maximum of 250.8 % at $T_{cond,out} = 70$ °C while S1 and S2 show similar values, except at lower temperatures ($T_{cond,out} \leq 65$ °C) where S2 performs best with a maximum efficiency of 289.0 % at the lowest supply tem-

perature (T_s = 55 °C) and condenser outlet temperature ($T_{cond,out}$ = 65 °C).

Because of the pumps electrical consumption, η_{tot} is lower than η_{th} to an extent which depends only on heat pump use and BTES charge as the STS and DH pumps operate in the same way across all scenarios. As reported in Table 3 and shown in Figure A.4, S3 experiences a larger drop from η_{th} compared to S1 and S2, resulting in S2 performing best for $T_{cond,out} \leq 75$ °C, S1 and S2 performing almost identically for $T_{cond,out} \geq 75$ °C) (with a slight advantage for S1). S3 performs worst due to increased pump consumption. Indeed in that case, the STS tank reaches high temperature more frequently (see Figure A.1), increasing the average condenser inlet temperature which, for a given temperature lift in the condenser, requires larger flow rates to deliver the same amount of heat. Therefore in the current circumstances, strategy S2 seems best suited in terms of thermal efficiency.

Finally, as expected, both the fuel costs and emissions are directly inversely correlated to η_{th} and η_{tot}, and therefore follow the same trends discussed above. With minima at [25.0,21.6,19.0] gCO2/kWh for supply temperatures of [75,65,55] °C with S2 scenario, the total emissions associated with heat generation and pumps are around 90 % below that of natural gas. Besides, in the same three S2 scenarios, operational costs are [4.1,20.5,34.2] % below that of natural gas (excluding pumps as they are not taken into account for gas). In general, both the emissions and operational costs are lowest with S2 and so are the total efficiencies.

Therefore from a consumer's perspective, the most beneficial option for maximal WF with the current system parameters appears to be S2 which achieves operational costs and emissions lower than that of gas. Together with the results on grid operator's benefits, S2 seems to be the best overall strategy given the current system parameters. However the capital costs, which are beyond the scope of this study, may remain prohibitively high due to the presence of large heat pumps and long-term thermal storage, and these results provide motivation for incentives and subsidies for the electrification of district heating networks with curtailed wind energy integration as it has the potential to lower the operational costs and emissions for the consumer, and utilise a significant amount of wind energy which would otherwise be curtailed if deployed at a large scale.

3.2.4. Supply temperature

The effect of the DHN supply temperature T_s has been described in the previous few paragraphs. As illustrated in Table 3, reducing T_s has a positive impact on all metrics of interest. Indeed, reducing T_s from 75 °C down to 55 °C for S2 increases the WF by up to 20 %, and reduces the total emissions and operational costs by up to 25 %. However as mentioned in section 1, a reduction in the DHN supply temperature must be accompanied by building retrofits, which may come at a significant cost. Therefore an additional cost analysis is necessary to weigh the gains in renewable energy and curtailed wind integration, operational costs and emissions against retrofit costs, which is beyond the scope of this work.

3.3. Sensitivity analysis

In this section, the impact of selected system parameters on the global system performance is analysed, such as not responding to curtailed wind (thereafter "Sens. 1"), the absence of BTES (thereafter "Sens. 2"), and a consumer discount on curtailed wind (thereafter "Sens. 3").

3.3.1. Not responding to curtailed wind

First, the case is analysed where the Operation Controller does not respond to curtailed wind. The main technical results are shown in Table 4 for strategy S2.

As expected, in all cases the WFs are significantly lower than for the base case (Table 3) by factors ranging from 53.3 % to 63.5 %. This highlights the system's flexibility and confirms the Operation Controller's ability to re-

INPUTS			OUTPUTS							
	T_s	$T_{cond,out}$	**WF, 6 MWe**	**WF loss**	η_{th}	η_{th}**, gain**	η_{tot}	η_{tot}**, gain**	γ_h	**Fuel cost reduction**
	°C	°C	%	%	%	%	%	MWe	%	%
	75	80	16.0	53.3	231.2	14.6	217.0	40.4	0.3	-
	75	85	16.0	56.2	206.0	12.3	196.1	37.0	0	-
	75	95	15.9	57.6	163.0	9.0	157.6	29.5	0	-
	65	70	15.9	57.8	291.3	19.6	270.1	52.3	0.8	-
Sens. 1	65	75	16.0	59.9	260.5	16.8	245.0	48.3	0.1	-
	65	95	15.9	60.7	163.2	7.9	158.1	29.4	0.1	-
	55	60	15.9	61.9	365.3	26.4	331.1	65.7	1.86	-
	55	65	16.0	63.5	329.4	23.6	305.0	62.7	0.1	-
	55	95	15.9	63.0	163.4	6.8	158.5	28.9	0	-
	75	80	29.8	13.1	206.9	2.6	190.2	23.0	-	17.8
	75	85	31.7	13.1	188.0	2.5	174.2	21.7	-	17.3
	75	95	32.5	13.3	153.7	2.8	144.1	18.4	-	14.8
	65	70	33.1	12.2	249.4	2.4	225.5	27.2	-	20.5
Sens. 2	65	75	34.8	12.8	228.6	2.5	208.1	26.0	-	19.0
	65	95	34.8	14.1	154.8	2.4	144.7	18.4	-	14.0
	55	60	36.9	11.5	295.9	2.4	262.7	31.5	-	23.2
	55	65	38.6	11.9	273.5	2.6	244.5	30.5	-	23.0
	55	95	36.4	15.3	155.6	1.7	145.2	18.0	-	14.1

Table 4: Summary of technical results for sensitivity test cases 1 ("Sens. 1", where the Operation Controller does not respond to wind) and 2 ("Sens. 2", without BTES). Results are presented for strategy S2 only. The "WF loss", "η_{th} gain" and "Fuel cost reduction" columns represents drops in wind fraction, efficiency improvements and fuel cost reductions from Table 3

spond to curtailed wind whilst meeting the load. Besides, the WFs take similar values across all scenarios, which is expected since curtailed wind energy shows no specific temporal pattern (see section 2.5.2).

The heater load is drastically reduced from the base case, and drops to zero in many cases, which confirms the heater's main role as boosting curtailed wind integration. It is still needed in some cases, particularly at low $T_{cond,out}$ with limited headroom as explained in section 3.1. As a consequence, the thermal efficiencies are between 6.8 % and 26.4 % larger, and the total efficiencies up to 65.7 % larger, to an extent which increases with decreasing $T_{cond,out}$. These results highlight the compromise between curtailed wind integration and thermal efficiency.

Such gains in efficiency cause fuel cost and emissions reductions (see Table 5), which further illustrates the compromise between curtailed wind integration and overall efficiency, with the former being beneficial to the grid operator, and the latter to the consumer. These results therefore highlight the need for curtailed wind integration incentives for consumers such as, for example, a market mechanism where a discount on curtailed wind energy is offered to the consumer. Such an option is explored in the "Sens. 3" sensitivity test case in section 3.3.3.

Finally, season-averaged electrical demand curves are shown in Figure 6 for all strategies, $T_s = 65$ °C, and $T_{cond,out} = 70$ °C. Compared to the base case, they are significantly flatter for S1 and S2, except for one early-

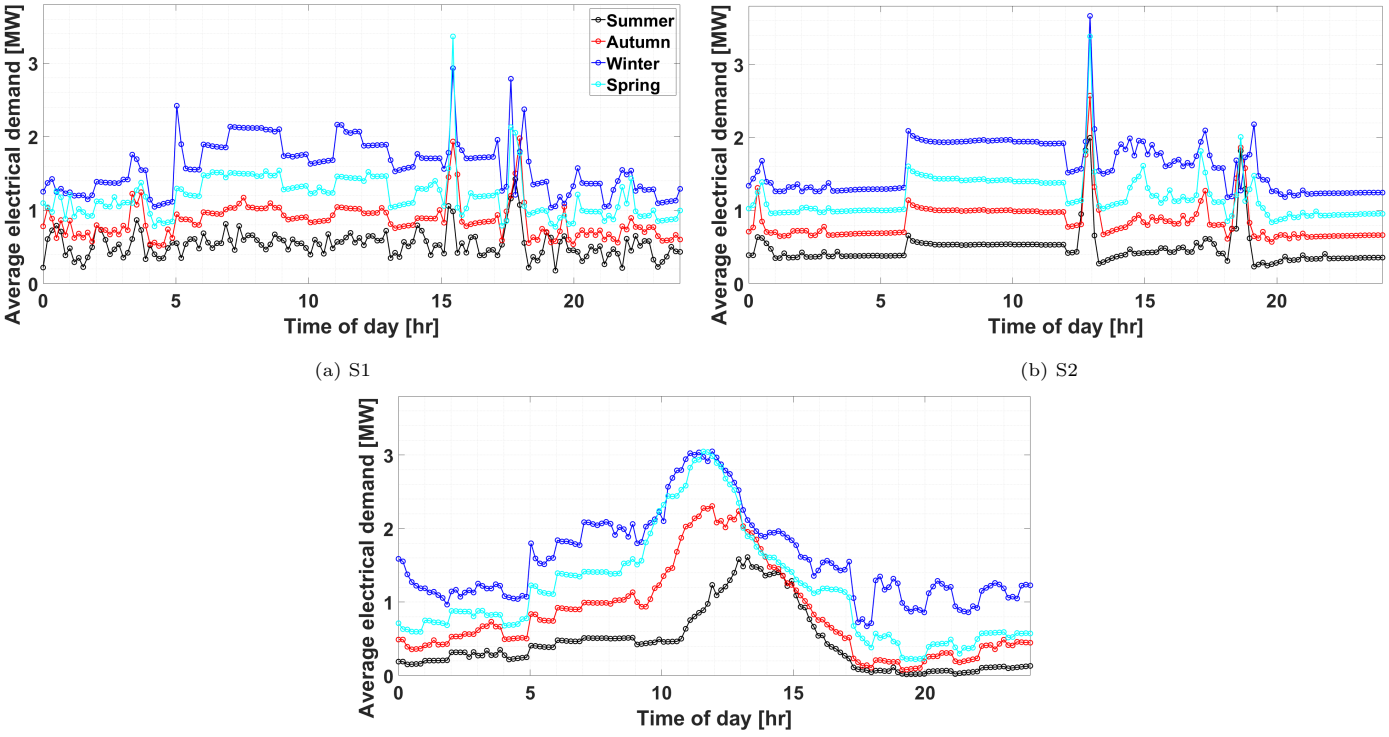

(a) S1

(b) S2

(c) S3

Figure 6: Season-averaged daily profiles for heat plant electrical consumption for heat generation for all strategies, $T_s = 65$ °C, $T_{cond,out} = 70$ °C and for the sensitivity test case where the Operation Controller does not respond to wind. The legend is the same for all graphs.

afternoon peak. Improvements are also observed for S3 in all seasons except winter, where the reduced electrical consumption at night time cannot be fully shifted to the hottest hours of the day given the restricted STS storage capacity. These results further illustrate the system's flexibility by its ability to respond to curtailed wind events and to provide load-levelling services, however they both appear to be limited by the STS tank capacity. This illustrates the interaction between different system parameters which must be considered during design.

3.3.2. Impact of BTES

Second, all scenarios with the S2 strategy are re-run with no BTES. The results are presented in Table 4.

The WFs are systematically lower without a BTES, with reductions ranging from 11.5 % to 15.3 %. However thermal efficiencies show a slight increase (maximum value 2.8 %) which is attributed to thermal losses from the BTES. But the total efficiencies (and, consequently, total fuel costs) show a more pronounced increase (by up to 31.5 %) as less pumping is required without a BTES.

Therefore, to the benefit of the grid operator, the BTES clearly allows higher levels of curtailed wind energy utilisation. However this comes at the expense of efficiency and cost, to the detriment of the consumer. This once more highlights the compromise between grid services and cost for the consumer which, as discussed in "Sens. 1" and "Sens. 3" (below), could be mitigated by the introduction of a market mechanism to incentivise the utilisation of curtailed wind, especially as levels are predicted to significantly rise in years to come. Moreover, a global multivariable optimisation study (as mentioned in the previous paragraph) where the BTES would be an optimisable variable may allow even greater levels of curtailed wind energy utilisation, which would increase the benefit of such a market mechanism (see Ref [28]).

3.3.3. Impact of a consumer discount on curtailed wind energy

Finally, in a third test case a 50 % discount on curtailed wind energy is considered, *i.e.* all curtailed wind energy is purchased at half of the Octopus Agile tariff. The results are shown in Table 5 for strategy S2.

As expected, the larger the total WF, the larger the cost reduction in the 50 % discount case, with average total cost reductions of 13.8 %. This is the expected value as total WFs are around 30 % so that a 50 % reduction yields a $0.3 \times 50 = 15$ % reduction ratio. Not responding to wind leads to total cost reductions proportional to total efficiency gains, with a 27.6 % average reduction.

These results show that, although not responding to wind remains cheaper in most cases reported above, comparable fuel costs are observed with a 50 % discount and large WFs. Fuel costs are therefore expected to further decrease with larger curtailed wind integration, which may be achieved with greater system flexibility, to an extent where it becomes cheaper to integrate large amounts of curtailed wind energy than not responding to it, which would be beneficial for both the grid operator and consumer. In addition, there is significant uncertainty in winter peak electricity prices for future decarbonisation scenarios with high shares of electrified heating. This again motivates further research into market mechanisms to incentivise curtailed wind integration as it could have a substantial impact on future curtailment levels in the UK and energy system efficiency as a whole if applied nationwide.

4. Conclusions

In this work, heat decarbonisation in the UK was addressed through an example case study of the University of Edinburgh's King's Buildings campus which has committed to carbon neutrality by 2040. The campus is currently fully reliant on gas for heat, with a 3$^{\text{rd}}$-generation DHN and a supply temperatures in excess of 85 °C in winter. To prevent a challenging retrofit to the campus buildings whilst decarbonising its heat supply, a heat pump based electrified heat plant design was proposed which operates at high supply temperatures and within the local grid connection restrictions. In addition, the heat plant's ability to provide grid services such as curtailed wind energy utilisation, demand-side flexibility and load-levelling was studied, and a long-term borehole thermal energy storage system was incorporated into the design. Three different control strategies were compared, and results were analysed from the perspective of the grid operator and consumer. The main findings of this paper are as follows:

- The control strategy, heat pump condenser outlet temperature and DHN supply temperature were found to have a great impact on the plant's overall efficiency and flexibility. In particular, a control strategy which minimises the STS tank SOC (like S1 and S2) was found to maximise the plant's load-levelling and curtailed wind integration ability
- From a grid operator's perspective, while all strategies showed great ability to respond to curtailed wind, strategy S2 was found to be best suited for load-levelling services whilst integrating curtailed wind energy, especially when the heat demand is highest, with WFs up to 43.8 %
- From a consumer's perspective, strategy S2 was also found to be the most beneficial with thermal and total efficiencies up to 289.0 % and 199.8 % respectively, and with equivalent fuel costs per unit energy lower than that of gas
- A clear compromise was highlighted between grid services (curtailed wind integration and load-levelling) and efficiency (*i.e.* operational costs), which are greatly influenced by the DHN supply temperature, heat pump output temperature, and the presence of a long-term thermal storage system
- Sensitivity test cases revealed that not responding to

		Base Case	50 % discount		No wind response (Sens. 1)	
T_s	$T_{cond,out}$	**Fuel cost, Total**	**Fuel cost, Total**	**Reduction from base case**	**Fuel cost, Total**	**Reduction from base case**
°C	°C	GBp/kWh	GBp/kWh	%	GBp/kWh	%
75	80	9.0	7.9	12.2	6.6	26.7
75	85	9.8	8.5	13.2	7.4	25.5
75	95	11.5	9.9	13.9	9.2	20.0
65	70	7.8	6.8	12.8	5.3	32.1
65	75	8.4	7.3	13.1	5.9	29.8
65	95	11.4	9.7	14.9	9.1	20.2
55	60	6.9	6.0	13.0	4.3	37.7
55	65	7.4	6.3	14.9	4.7	36.5
55	95	11.3	9.5	15.9	9.1	19.5

Table 5: Fuel costs for the base case alongside the cases of a 50 % discount on wind energy, and no wind response (Strategy S2). The cost reductions from the base case are also indicated

curtailed wind could improve total efficiencies and total fuel costs by more than 26 % and 37 % respectively. But it was also shown that a 50 % discount on curtailed wind energy for the consumer could significantly lower operational costs to an extent which grows with WFs, so that with larger WFs integrating curtailed wind energy may become cheaper than not responding to it, which would benefit both the grid operator and consumer. These results therefore provide motivation for further research into market mechanisms to incentivise curtailed wind integration as it could have a substantial impact on future curtailment levels in the UK and energy system efficiency as a whole if applied at a large scale

- Reducing the DHN supply temperature was found to have a positive impact on all metrics of interest. For example a reduction from 75 °C down to 55 °C leads to a 20 % WF increase and cost and emissions reductions up to 25 %. However such improvements must be balanced again the costs of building retrofits which would be necessary to maintain the same level of thermal comfort

Finally, the work presented in this paper may be complemented in several ways. For example:

- Investigating the impact of a market mechanism to incentivise curtailed wind integration on future curtailed wind levels, global energy system's efficiency and consumer benefit. This could be integrated into a global multi-variable optimisation study of the heat plant design proposed in this work, with considerations of capital and maintenance costs, and has been done elsewhere [28]

- The financial impact of lowering the DHN supply temperature could be balanced against that of a retrofit which would be required to maintain the same level of thermal comfort

- Other curtailment wind levels must be investigated as they are predicted to significantly increase over the next decade, which could substantially improve the grid services and benefits of the heat plant design presented in this study

- Electrifying the whole country for both power and heat may be difficult, and it may be necessary to investigate other storage technologies and heat sources for the decarbonisation of heat such as waste heat and solar power, and how they could be integrated alongside the one presented in this work for a faster and

more efficient decarbonisation of the heat sector as a whole

Acknowledgments

This work was funded by the INTEGRATE (EPSRC grant number EP/T023112/1) and HEAT BALANCE (Strategic Innovation Fund Grant number 10037467) projects. For the purpose of open access, the authors have applied a Creative Commons Attributions (CC BY) licence to any Author Accepted Manuscript version arising from this submission.

References

[1] Scottish Energy Statistics Hub, accessed 28/03/2023. URL https://scotland.shinyapps.io/Energy/?Section=WholeSystem&Chart=RenEnTgt

[2] R. Renaldi, D. Friedrich, Techno-economic analysis of a solar district heating system with seasonal thermal storage in the UK, Applied Energy 236 (2019) 388–400.

[3] S. A. Maximov, D. Friedrich, Multi-objective optimisation of a solar district heating network with seasonal storage for conditions in cities of southern Chile, Sustainable Cities and Society 73 (2021).

[4] A. Lyden, C. S. Brown, I. Kolo, G. Falcone, D. Friedrich, Seasonal thermal energy storage in smart energy systems: District-level applications and modelling approaches, Renewable and Sustainable Energy Reviews 167 (2022).

[5] J. Rosenow, Is heating homes with hydrogen all but a pipe dream?, Joule 6 (2022) 2219–2239.

[6] Modelling borehole thermal energy storage using curtailed wind energy as a fluctuating source of charge, 48th Workshop on Geothermal Reservoir Engineering, Stanford.

[7] National Grid ESO, Future Energy Scenarios (2022).

[8] L. Gao, J. Zhao, Z. Tang, A review on borehole seasonal solar thermal energy storage, Energy Procedia 70 (2015) 209–218. doi:https://doi.org/10.1016/j.egypro.2015.02.117.

[9] H. Skarphagen, D. Banks, B. S. Frengstad, H. Gether, Design considerations for borehole thermal energy storage (btes): a review with emphasis on convective heat transfer, Geofluids 2019 (2019). doi:https://doi.org/10.1155/2019/4961781.

[10] M. Reuss, 6 - the use of borehole thermal energy storage (btes) systems, in: L. F. Cabeza (Ed.), Advances in Thermal Energy Storage Systems, Woodhead Publishing Series in Energy, Woodhead Publishing, 2015, pp. 117–147.

[11] M. Malmberg, W. Mazzotti, J. Acuna, H. L. A. Lindstahl, High-temperature borehole thermal energy storage - A case study, in: IGSHPA Research Track, 2018.

[12] L. Hermans, R. Haesen, A. Uytterhoeven, W. Peere, W. Boydens, L. Helsen, Pre-design of collective residential solar districts with seasonal thermal energy storage: Importance of level of detail, Applied Thermal Engineering 226 (2023).

[13] Monitoring results from large scale heat storages for district heating in Denmark, 14th International Conference on Energy Storage, Adana.

[14] L. Mesquita, D. McClenahan, J. Thornton, J. Carriere, B. Wong, Drake Landing Solar Community: 10 years of operation, in: ISES Solar World Congress 2017, 2017. doi:https://doi.org/10.18086/swc.2017.06.09.

[15] N. Gohl, D. Bauer, H. Drück, 1to10 - a cost-effective heat supply concept with low primary energy consumption for multi-family houses and small residential areas, Energy Procedia 91 (2016) 460–466. doi:https://doi.org/10.1016/j.egypro.2016.06.179.

[16] D. Bauer, W. Heidemann, H.-J. Diersch, Transient 3d analysis of borehole heat exchanger modeling, Geothermics 40 (4) (2011) 250–260. doi:https://doi.org/10.1016/j.geothermics.2011.08.001.

[17] H.-J. G. Diersch, D. Bauer, 7 - analysis, modeling, and simulation of underground thermal energy storage systems, in: L. F. Cabeza (Ed.), Advances in Thermal Energy Storage Systems (Second Edition), second edition Edition, Woodhead Publishing Series in Energy, Woodhead Publishing, 2021, pp. 173–203. doi:https://doi.org/10.1016/B978-0-12-819885-8.00007-3.

[18] H.-J. Diersch, D. Bauer, W. Heidemann, W. Rühaak, P. Schätzl, Finite elements modeling of borehole heat exchanger systems Part 1. Fundamentals, Computers & Geosciences 37 (2011). doi:10.1016/j.cageo.2010.08.003.

[19] S. Lanini, F. Delaleux, X. Py, R. Olives, D. Nguyen, Improvement of borehole thermal energy storage design based on experimental and modelling results, Energy and Buildings 77 (2014) 393–400.

[20] D. Pahud, G. Hellström, The new duct ground heat model for TRNSYS, eurotherm. Physical Models for Thermal Energy Stores, Eindhoven (1996).

[21] H. Lund, S. Werner, R. Wiltshire, S. Svendsen, J. E. Thorsen, F. Hvelplund, B. V. Mathiesen, 4th generation district heating (4gdh): Integrating smart thermal grids into future sustainable energy systems, Energy 68 (2014) 1–11. doi:https://doi.org/10.1016/j.energy.2014.02.089.

[22] S. Buffa, M. Cozzini, M. D'Antoni, M. Baratieri, R. Fedrizzi, 5th generation district heating and cooling systems: A review of existing cases in europe, Renewable and Sustainable Energy

Reviews 104 (2019) 504–522. doi:https://doi.org/10.1016/j.rser.2018.12.059.

[23] O. Angelidis, A. Ioannou, D. Friedrich, A. Thomson, G. Falcone, District heating and cooling networks with decentralised energy substations: Opportunities and barriers for holistic energy system decarbonisation, Energy 269 (2023) 126740. doi:https://doi.org/10.1016/j.energy.2023.126740.

[24] D. Schmidt, A. Kallert, M. Blesl, S. Svendsen, H. Li, N. Nord, K. Sipilä, Low temperature district heating for future energy systems, Energy Procedia 116 (2017) 26–38, 15th International Symposium on District Heating and Cooling, DHC15-2016, 4-7 September 2016, Seoul, South Korea. doi:https://doi.org/10.1016/j.egypro.2017.05.052.

[25] A. Volkova, I. Krupenski, H. Pieper, A. Ledvanov, E. L. ošov, A. Siirde, Small low-temperature district heating network development prospects, Energy 178 (2019) 714–722. doi:https://doi.org/10.1016/j.energy.2019.04.083.

[26] M. Brand, S. Svendsen, Renewable-based low-temperature district heating for existing buildings in various stages of refurbishment, Energy 62 (2013) 311–319. doi:https://doi.org/10.1016/j.energy.2013.09.027.

[27] D. S. Østergaard, S. Svendsen, Replacing critical radiators to increase the potential to use low-temperature district heating – A case study of 4 Danish single-family houses from the 1930s, Energy 110 (2016) 75–84. doi:https://doi.org/10.1016/j.energy.2016.03.140.

[28] T. Desguers, A. Lyden, D. Friedrich, Integration of curtailed wind into flexible electrified heating networks with demand-side response and thermal storage: Practicalities and need for market mechanisms, Energy Conversion and Management 304 (2024). doi:https://doi.org/10.1016/j.enconman.2024.118203.

[29] P. Sorensen, T. Schmidt, Design and constructio of large scale heat storages for distring heating in Denmark, in: 14th International Conference on Energy Storage, Adana, 2018.

[30] Elexon portal, accessed in 2020.
URL https://www.elexonportal.co.uk/news/latest?cachebust=wa8dva0cpq

[31] D. Friedrich, EnergySystemData, accessed 3rd April 2023.
URL https://github.com/DrDanielFriedrich/EnergySystemData

[32] National Grid ESO. Carbon Intensity API, Envirionmental Defense Fund Europe, University of Oxford, WWF. Accessed August 2022.
URL https://www.carbonintensity.org.uk/

[33] Energy Stats UK. Octopus Agile, accessed August 2022.
URL https://energy-stats.uk/octopus-agile/

[34] Forest Research. Tools and Resources: Carbon emissions of different fuels, accessed January 2023.
URL https://www.forestresearch.gov.uk/tools-and-resources/fthr/biomass-energy-resources/reference-biomass/facts-figures/carbon-emissions-of-different-fuels

Appendix A. Supporting information

Supporting graphs

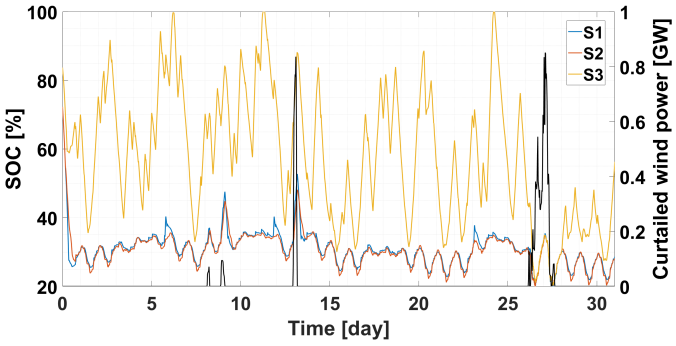

Figure A.1: STS SOC for a winter month during low wind curtailment levels (8th January - 8th February) for all three strategies, $T_s = 65$ °C and $T_{cond,out} = 95$ °C

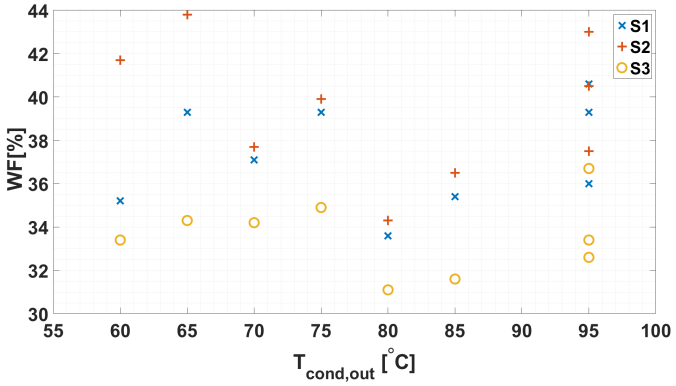

Figure A.2: WF (excluding pumps) as reported in Table 3

BTES parameters

Parameter	Unit	Value	Parameter	Unit	Value
STS volume	m^3	2,000	BTES U-tube shank	m	0.0475
ASHP	MWe	1-6	Number of parallel strings	-	41
STS electric heater power	MWe	0-6	Number of boreholes per string	-	6
T_s	°C	[55,65,75]	Ground thermal conductivity	W/m/K	2.25
T_r	°C	$T_s - 20$	Ground volumetric heat capacity	$J/m^3/K$	$2.2 \cdot 10^6$
$T_{cond,out}$	°C	$T_s + 5$:95[a]	Grout thermal conductivity	W/m/K	0.89
Grid connection	MWe	6	Pipes (PEX) thermal conductivity	W/m/K	0.41
BTES depth	m	60	Circulation pumps rated MFR	kg/s	80
BTES radius	m	16.5	STS and DH pumps rated MFR	kg/s	$2525.5/(T_s - T_r)$
BTES ground area	m^2	854.9	BTES pump rated MFR	kg/s	98.4
BTES volume	m^3	51,291.9	BTES maximum allowed temperature	°C	95
Number of boreholes	-	246	Pipe roughness ϵ	mm	0.015
Borehole spacing	m	2	Water density	kg/m^3	999
Borehole diameter	m	0.2	Water specific heat	J/kg/K	4190
BTES U-tube pipe inner diameter	m	0.05	DHN pipes length	m	1,500
BTES U-tube pipe thickness	m	0.0025			

[a] In increments of 5°C

Table A.1: Design parameters and their values (from Ref [28], with additional parameters). MFR stands for mass flow rate

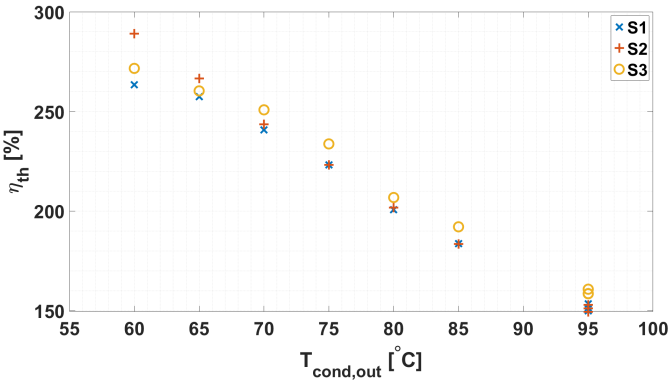

Figure A.3: η_{th} efficiencies as reported in Table 3

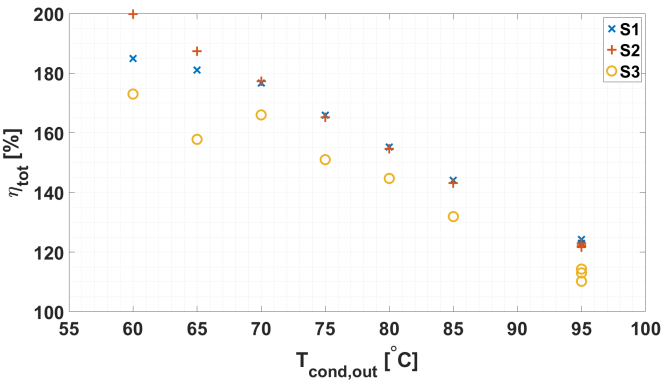

Figure A.4: η_{tot} efficiencies as reported in Table 3